

Spectral Energy Distributions and Age Estimates of 172 Globular Clusters in M31

Linhua Jiang^{1,2}, Jun Ma¹, Xu Zhou¹, Jiansheng Chen¹, Hong Wu¹, and Zhaoji Jiang¹

Received _____; accepted _____

¹National Astronomical Observatories of CAS and CAS-Peking University joint Beijing
Astrophysical Center, Beijing, 100012, P. R. China

²Department of Astronomy, Peking University, Beijing, 100871, P. R. China

ABSTRACT

In this paper we present CCD multicolor photometry for 172 globular clusters (GCs), taken from the Bologna catalog (Battistini et al. 1987), in the nearby spiral galaxy M31. The observations were carried out by using the National Astronomical Observatories 60/90 cm Schmidt Telescope in 13 intermediate-band filters, which covered a range of wavelength from 3800 to 10000Å. This provides a multicolor map of M31 in pixels of $1.^{\prime\prime}7 \times 1.^{\prime\prime}7$. By aperture photometry, we obtain the spectral energy distributions (SEDs) for these GCs. Using the relationship between the BATC intermediate-band system used for the observations and the *UBVRI* broad-band system, the magnitudes in the *B* and *V* bands are derived. The computed *V* and *B* – *V* are in agreement with the values given by Battistini et al. (1987) and Barmby et al. (2000). Finally, by comparing the photometry of each GC with theoretical stellar population synthesis models, we estimate ages of the sample GCs for different metallicities. The results show that nearly all our sample GCs have ages more than 10^9 years, and most of them are around 10^{10} years old. Also, we find that GCs fitted by the metal-poor model are generally older than ones fitted by the metal-rich model.

Subject headings: galaxies: individual (M31) – galaxies: evolution – galaxies: globular clusters

1. INTRODUCTION

The study of globular clusters (GCs) plays an important role in our understanding of the evolution and structure of galaxies. A single globular cluster is a “packet” of population II stars with a single age and chemical abundance, so the GCs provide a unique laboratory for exploring dynamics and theoretical evolution of their parent galaxies. GCs are likely to be the oldest known stellar objects, and all large galaxies appear to contain them (Harris 1991). Among the Local Group galaxies, M31 is an ideal target for studying GCs, since it comprises the largest sample of GCs, which is more than all GCs combined in other Local Group members (Battistini et al. 1987; Racine 1991; Harris 1991; Fusi Pecci et al. 1993). It is thus well known that the understanding of M31 GCs is especially important.

M31, a large spiral galaxy, is one of our nearest neighbors, with a distance modulus of 24.47 (Holland 1998; Stanek & Garnavich 1998). Because it is so near, and has a very large sample of GCs, M31 is an excellent candidate for GCs studies. The first catalog of 140 clusters in M31 was given by Hubble (1932). From then on, numerous lists of GC candidates were published. A general catalog of almost all the GCs known in the early time was compiled by Vetešnik (1962a), who gave a total number of 257 GCs, including most candidates identified by previous works (e.g. Hubble 1932; Seyfert & Nassau 1945; Hiltner 1958; Mayall & Eggen 1953; Kron & Mayall 1960). Later, several major catalogs were compiled by Sargent et al. (1977), Crampton et al. (1985), and Bologna Group (Battistini et al. 1980, 1987). Sargent et al. (1977) found or confirmed 355 GCs in their catalog, and also rejected 52 candidates obtained by previous surveys. The catalog of Crampton et al. (1985) was a compilation with 509 GC candidates, and the core radii, V magnitudes, and intrinsic colors for most candidates were also given or estimated. The most comprehensive catalog of globular cluster candidates may be the Bologna catalog (Battistini et al. 1987). Bologna Group did independent searches for candidates and compiled them with their own Bologna number. Bologna catalog contains a total of 827 objects, and all the objects were classified into five classes by authors’ degree of confidence. 353 of these candidates were considered as class A or class B by high level of confidence, and the others fell into class C, D, or E. V

magnitude and $B - V$ color for most candidates were also given in the Bologna catalog.

All globular cluster candidates in these catalogs were sure carefully selected and usually identified by several steps. However, it is not to say that these samples were clean. They were often contaminated by foreground stars, background galaxies, or other objects (e.g. HII regions). For example, even several class A, or B candidates in Bologna catalog turned out to be not GCs (Barmby et al. 2000). Similarly, these catalogs were not complete, although they may be fairly complete down to $V = 18$ ($M_v \sim -6.5$) (Fusi Pecci et al. 1993). Actually, most candidates in Bologna catalog also reached down to $V = 18$ (Battistini et al. 1987). So in recent years, many works were searching for new and fainter GCs, especially in the center region of M31(e.g. Aurière, Coupinot, & Hecquet 1992; Battistini et al. 1993). Additionally, some much fainter GCs were detected by *HST* with high spatial resolution (e.g. Barmby & Huchra 2001a; Rich et al. 2001). According to the estimate of Barmby & Huchra (2001a), the total number of GCs in M31 is about 460 ± 70 .

Anyway, these samples provide a good database for studies of M31 GCs. On the basis of the database, many results were derived and some properties of M31 GCs were well explored, such as luminosity function (e.g. Aurière, Coupinot, & Hecquet 1992; Mochejska et al. 1998; Barmby, Huchra, & Brodie 2001b), reddening and intrinsic colors (e.g. Vetešnik 1962b; Bajaja & Gergely 1977; Iye & Richter 1985; Barmby et al. 2000), metallicities (e.g. van den Bergh 1969; Ashman & Bird 1993; Barmby et al. 2000; Perrett et al. 2002), and comparisons with the Galactic GCs and M33 GCs (e.g. Hiltner 1960; Frogel, Persson, & Cohen 1980; Reed, Harris, & Harris 1992; Mochejska et al. 1998).

Although there are already much observation information and theoretical results in previous studies, for full physical information about the GCs, it is of great value to obtain multiband photometry, which can provide their accurate SEDs. In addition, we can estimate GC ages by comparing their intrinsic SEDs with ones of theoretical stellar population synthesis models. The globular cluster ages are important, they can provide us with information on the early formative stages of the parent galaxy and can be utilized to provide a lower limit to the age of the parent galaxy. Especially, the distribution of GC ages can

be used to understand the conditions for their formation. For example, Barmby & Huchra (2000) presented that conditions for cluster formation must have existed for a substantial fraction of the parent galaxy’s lifetime by comparing three sets of population synthesis models with integrated colors of M31 and Galactic globular clusters in set of *UBVRIJHK*. However, ages of most individual GCs in M31 remain undetermined, although they have been derived for a few ones. For example, Jablonka, Alloin, & Bica (1992) presented spectrophotometric data for 7 GCs, and derived their reddening, metallicities and ages. According to the calculation of Borges and Idiart (1995), de Freitas Pacheco (1997) reported a sample of 12 GCs, and obtained the mean age of the sample.

In this paper we present CCD spectrophotometry of a set of GCs in M31 using images obtained with the Beijing-Arizona-Taiwan-Connecticut (BATC) Multicolor Sky Survey Telescope designed to obtain SED information for galaxies (Fan et al. 1996). The BATC system uses the 60/90 cm Schmidt telescope with 15 intermediate bandwidth filters. In this study we use 13 of these filters, from 3800 to 10000Å, with images covering the most visible extent of M31, and present the SEDs of 172 GCs selected from the Bologna catalog (Battistini et al. 1987). Using previously derived relationships between the BATC intermediate-band system, we go on to compute the *B* and *V* magnitudes for these objects. The computed *V* magnitudes and *B* – *V* colors are in good agreement with the values given by Battistini et al. (1987) and Barmby et al. (2000). We also plot histograms of the *V* band magnitudes and of *B* – *V* colors, as well as plotting the corresponding color-magnitude diagram for our sample GCs. Since reddening of GCs in M31 was determined by several authors (e.g. Vetešnik 1962b; Crampton et al. 1985; Barmby et al. 2000), we can infer the intrinsic colors for each individual GC. Finally, using theoretical stellar population synthesis models, we estimate ages of our sample GCs. The results show that most objects are as old as about 10^{10} years, and GCs fitted by the metal-poor model are generally older than ones fitted by the metal-rich model.

This paper will take the following form: Section 2 presents our sample GCs, and details of observations and data reduction. We also obtain SEDs, and give comparisons of GC photometry between the BATC system and previous measurements in this section. In

Section 3, we briefly describe the stellar population synthesis models of GSSP. We present how we deredden the sample GCs in Section 4. In Section 5, ages for the GCs are estimated for different values of metallicity. Finally, we give a summary in Section 6.

2. SAMPLE OF GLOBULAR CLUSTERS, OBSERVATIONS AND DATA REDUCTION

2.1. Selection of Sample

The GC candidates in each catalog were sure carefully selected and identified by different ways or several steps, however, the catalogs of GCs were often contaminated by stars, background galaxies, or other objects such as HII regions. The basic idea of the identification of a new GC candidate is the fact that the point spread function (PSF) of a GC has a larger FWHM than a star (Mochejska et al. 1998). In general, people discover a new GC first using visual inspection, i.e., distinguish cluster images from stars or spurious non-stellar objects by image morphology (Battistini et al. 1987). For example, objects that appear asymmetrical or exhibit structure are usually not GCs, thus most open clusters and background galaxies which are asymmetrical or display structure are easy to be eliminated (Crampton et al. 1985). Sometimes identifying a new GC in the center region or in the halo of M31 need other means. Due to the strong background gradient, the identification of candidates in the center region by image morphology may be less efficient. Aurière et al. (1992) used another powerful method, the wavelet analysis, to reduce the image. For the candidates in the M31 halo, there are also several other ways to define a clean sample (see Reed, Harris, & Harris 1992 for a detail).

The sample of GCs chosen in this paper is from the Bologna catalog by Battistini et al. (1987). As has been mentioned, the Bologna catalog with a total of 827 GC candidates, is the most comprehensive catalog of M31 GCs. All the candidates were classified into five classes by authors' degree of confidence. 353 of all the candidates were considered as class A (254 objects) and class B (99 objects) by very high and high level of confidence, 152 candidates were listed in class C, and the others fell into class D and E. Our selection of

the sample is as follows. First, we take all candidates of class A and B (i.e. Table IV of Bologna catalog) as our original sample. We find that only 223 objects are in our CCD field. Then we note that cluster 7, 55, 132 and 147 are virtually stars, not true GCs (Barmby et al. 2000), so they are not included in our sample, i.e., there are 219 class A or B GCs of Bologna catalog in our CCD field. Besides, 47 of 219 GCs, which are saturated in some filters, are also excluded in our sample. At last 172 GCs are included here. Since our sample candidates in Bologna catalog are classified into class A and B by authors' high level of confidence, and cross-checked by others (e.g. Barmby et al. 2000), we consider that these objects are GCs, and we do not confirm them again. In addition, we should emphasize that the numbering system of the Bologna catalog is adopted in this paper.

2.2. Observations and Data Reduction

The large field multicolor observations of M31 were obtained in the BATC photometric system, in which a 60/90 cm f/3 Schmidt telescope is used. This telescope is located at Xinglong Station of National Astronomical Observatories. A Ford Aerospace 2048×2048 CCD camera, with 15 μm pixel size is mounted at the Schmidt focus, giving a CCD field of view of $58' \times 58'$ with a pixel size of $1''7$.

The multiband BATC filter system comprises 15 intermediate-band filters, covering the full optical wavelength range from 3000 to 10000Å. The filters were designed specifically to avoid contamination from the brightest and most variable night sky emission lines. Details of the Schmidt Telescope, the CCD camera, the data acquisition system, and the definition of the BATC filter passbands can be found in previous publications (Fan et al. 1996; Zheng et al. 1999). The observations of M31 were carried out from September 15, 1995, through December 16, 1999, with a total exposure time of about 37 hr 20 min, while the CCD images were accumulated in 13 of the BATC filters. The dome flats were obtained using a diffusor plate in front of the Schmidt corrector plate. For flux calibration the Oke-Gunn primary standard stars HD 19445, HD 84937, BD $+26^{\circ}2606$, and BD $+17^{\circ}4708$ were observed under photometric conditions (see Yan et al. 2000, Zhou et al. 2001 for details). The parameters

of the filters, and the basic statistics of the observations are given in Table 1.

Using standard procedures, the data were reduced by automatic reduction software: PIPELINE I, which include bias subtraction and flat-fielding of the CCD images. This software was developed for the BATC multicolor sky survey (see Ma et al. 2001, 2002a for a detail). The absolute flux of images was calibrated using observations of standard stars. Fluxes, as observed through the BATC filters for the Oke-Gunn stars, were derived by convolving the SEDs of these stars with the measured BATC filter transmission functions (Fan et al. 1996). In Table 1, *Column 6* gives the zero point errors in magnitude for the standard stars through each filter. The formal errors obtained for these stars in the 13 BATC filters used are $\lesssim 0.02$ mag, which implies that we can define photometrically the BATC system to an accuracy of better than 0.02 mag.

2.3. Integrated Photometry

To obtain the magnitude of a given GC, the PHOT routine in DAOPHOT (Stetson 1987, 1990) is used. For avoiding contamination from nearby objects, We adopt a small aperture diameter of $10''.2$, which corresponds to a diameter of 6 pixels in Ford CCDs. Aperture corrections are computed using isolated stars. Finally we obtained the SEDs in 13 BATC filters for 172 GCs, which are listed in Table 2. The table contains the following information: *Column 1* is the cluster number taken from the Bologna catalog (Battistini et al. 1987). *Column 2* to *Column 14* present the magnitudes in the selected BATC bands, and on a second row for each GC in these columns we give the magnitude uncertainty for each band. The uncertainties are given by DAOPHOT.

2.4. Magnitudes in the *B* and *V* Bands, and *B* – *V* Colors

Using Landolt standards and the catalogs of Landolt (1983, 1992) and of Galadí-Enríquez et al. (2000), Zhou et al. (2002) derived the relationships between the BATC intermediate band system and the *UBVRI* broad-band system. These relationships are

Table 1: Parameters of the BATC Filters and Statistics of Observations

No.	Name	cw ^a (Å)	Exp. (hr)	N.img ^b	rms ^c
1	BATC03	4210	01:00	03	0.015
2	BATC04	4546	05:30	17	0.009
3	BATC05	4872	03:30	11	0.015
4	BATC06	5250	02:20	12	0.006
5	BATC07	5785	02:15	07	0.003
6	BATC08	6075	01:40	05	0.003
7	BATC09	6710	00:45	03	0.003
8	BATC10	7010	03:00	12	0.008
9	BATC11	7530	02:00	06	0.004
10	BATC12	8000	04:00	12	0.003
11	BATC13	8510	01:30	05	0.004
12	BATC14	9170	05:50	18	0.003
13	BATC15	9720	04:00	12	0.009

^aCentral wavelength for each BATC filter

^bImage numbers for each BATC filter

^cZero point error, in magnitude, for each filter as obtained from the standard stars

given in equations (1) and (2) as:

$$m_B = m_{04} + (0.2218 \pm 0.033)(m_{03} - m_{05}) + 0.0741 \pm 0.033, \quad (1)$$

$$m_V = m_{07} + (0.3233 \pm 0.019)(m_{06} - m_{08}) + 0.0590 \pm 0.010. \quad (2)$$

Using equations (1) and (2) we transformed the magnitudes of the 172 GCs in the BATC03, BATC04 and BATC05 bands into *B* band magnitudes, and also derived *V* band magnitudes from those in BATC06, BATC07 and BATC08.

Histograms of the computed *V* magnitudes and *B* – *V* colors, and color-magnitude diagram, *V* against *B* – *V*, are shown in Figure 1. The figure is in good agreement with the

corresponding plots of class A and B GCs given by Battistini et al. (1987). From the left panel of Figure 1 we can see that most of our sample GCs are brighter than $V = 18$. This relates to the original catalog, because V magnitudes of most class A and B GCs in Bologna catalog are brighter than 18 mag. The right panel of Figure 1 shows that $B - V$ colors of most GCs are redder than 0.6, which is reasonable. Actually, the GCs are generally the objects with $B - V > 0.6$ (Crampton et al. 1985) or $B - V > 0.55$ (Barmby et al. 2000). Iye & Richter (1985) even considered $B - V < 0.6$ as one of their criteria of rejecting GC candidates.

We also present the comparisons of the BATC photometry with previously published measurements (Battistini et al. 1987; Barmby et al. 2000) in Figures 2 and 3. These figures do not present all GCs of our sample, since V magnitudes and $B - V$ colors of some GCs were not given by Battistini et al. (1987) and Barmby et al. (2000). Figure 2 plots the comparison for 157 objects, while Figure 3 for 141 objects. From these figures, it can be seen that there are good agreements between the BATC photometry and the other two photometric measurements. In Figure 2, the differences of V magnitudes for several objects are abnormally big, such as clusters 118, 127, 131, 138, and 186. The reason may be that clusters 118, 127, 131 and 138 lie in the center region of the parent galaxy, so we can not subtract the background very well. However, the BATC V magnitude of cluster 186 is in good agreement with the value presented by Barmby et al. (2000). The mean differences of V and $B - V$ between the BATC photometry and Battistini et al. (the BATC photometric values minus the values of Battistini et al.) are $\langle \Delta V \rangle = -0.083 \pm 0.069$ and $\langle \Delta(B - V) \rangle = -0.128 \pm 0.096$ (excluding objects mentioned above), and between the BATC photometry and Barmby et al. (2000) are $\langle \Delta V \rangle = 0.063 \pm 0.065$ and $\langle \Delta(B - V) \rangle = 0.067 \pm 0.090$, respectively. The uncertainties in B (BATC) and V (BATC) were determined linearly, i.e. $\sigma_B = \sigma_{04} + 0.2218(\sigma_{03} + \sigma_{05})$ and $\sigma_V = \sigma_{07} + 0.3233(\sigma_{06} + \sigma_{08})$, to reflect photometric errors in the six filter bands. For the colors, we calculated their errors by $\sigma_{B-V} = \sqrt{\sigma_B^2 + \sigma_V^2}$. From these two figures, we can see that, our results are in better agreement with Barmby et al. (2000) than with Battistini et al. (1987).

3. DATABASES OF SIMPLE STELLAR POPULATIONS

A simple stellar population (SSP) is defined as a single generation of coeval stars with fixed parameters such as metal abundance, initial mass function, etc. (Buzzoni 1997). In evolutionary synthesis models, they are modeled by a collection of evolutionary tracks of stars with different masses and initial chemical components, and a set of stellar spectra at different evolutionary stages. Because SSPs are the basic building elements for synthetic spectra of galaxies, we can infer the formation and evolution of the parent galaxies from them (Jablonka et al. 1996). Since Tinsley (1972) and Searle et al. (1973) did the pioneering work in evolutionary population synthesis, this method has become a standard technique to study the stellar populations of galaxies. A broad variety of empirical and theoretical database has been built up, and a comprehensive library of models has been compiled (Leitherer et al. 1996). Widely used models are from GISSEL96 (Charlot & Bruzual 1991; Bruzual & Charlot 1993; Bruzual & Charlot 1996, unpublished), the Padova and Geneva group (e.g. Schaerer & de Koter 1997; Schaerer & Vacca 1998; Bressan et al. 1996; Chiosi et al. 1998), PEGASE (Fioc & Rocca-Volmerange 1997) and STARBURST99 (Leitherer et al. 1999).

In present paper, we will use the SSPs of Galaxy Isochrone Synthesis Spectra Evolution Library (hereafter GSSP; Bruzual & Charlot 1996, unpublished) to estimate the ages of the sample GCs, since they are simple and well explored.

3.1. Spectral Energy Distribution of GSSPs

GSSPs method, which is based on a model of stellar population synthesis developed by Charlot & Bruzual (1991), can be used to determine the distribution of stars in the theoretical color-magnitude diagram for any stellar system. The updated GSSPs synthesis model (Bruzual & Charlot 1996, unpublished), which upgraded from the Bruzual & Charlot (1993) version, provides the evolution of the spectra photometric properties for a wider range of stellar metallicities, with $Z = 0.0004, 0.004, 0.008, 0.02, 0.05$, and 0.1 . The chemical parameters follow the helium-to-metal enrichment law $dY/dZ = 2.5$, and the

initial mass function obeys the Salpeter (1955) law with $\alpha = 2.35$ (Leitherer et al. 1996).

3.2. Integrated Colors of GSSPs

To obtain the age, metallicity, and interstellar-medium reddening distribution for M81, Kong et al. (2000) found the best match between the intrinsic colors and the predictions of GSSP for each cell of M81. To estimate the ages for the sample clusters in this paper, we follow the method of Kong et al. (2000). Since the observational data are integrated luminosity, as Kong et al. (2000) and Ma et al. (2002b) did, we convolve the SED of GSSP with the BATC filter profiles to obtain the optical and near-infrared integrated luminosity for comparisons. The integrated luminosity $L_{\lambda_i}(t, Z)$ in the i th BATC filter can be calculated with

$$L_{\lambda_i}(t, Z) = \frac{\int F_\lambda(t, Z) \varphi_i(\lambda) d\lambda}{\int \varphi_i(\lambda) d\lambda}, \quad (3)$$

where $F_\lambda(t, Z)$ is the SED of the GSSP of metallicity Z at age t , and $\varphi_i(\lambda)$ is the response function in the i th filter of the BATC filter system ($i = 3, 4, \dots, 15$), respectively. To avoid using parameters that are dependent on the distance, we calculate the integrated colors of a GSSP relative to the BATC filter BATC08 ($\lambda = 6075\text{\AA}$):

$$C_{\lambda_i}(t, Z) = L_{\lambda_i}(t, Z)/L_{6075}(t, Z). \quad (4)$$

Finally, using equations (3) and (4) we obtained the intermediate-band colors of a GSSP for six metallicities from $Z = 0.0004$ to $Z = 0.1$.

4. REDDENING CORRECTION

The SED of a stellar system will be affected by age, metallicity and reddening along the line of sight. Generally, older age, higher metallicity and larger reddening all lead to redder SEDs of stellar systems in the optical (Bressan, Chiosi, & Tantalo 1996; Mollà, Ferrini, & Diaz 1997), and these effects are difficult to separate (Calzetti 1997; Vazdekis et al. 1997; Origlia et al. 1999). In order to estimate the ages for 172 GCs, the intrinsic colors

of these GCs should be obtained. The observed colors are mainly affected by two sources of reddening: the foreground extinction in the Milk Way and internal reddening in M31.

The Galactic reddening in the direction of M31 was estimated by many authors (e.g. van den Bergh 1969; McClure & Racine 1969; Frogel, Persson, & Cohen 1980), and the similar values of the foreground color excess, $E(B - V)$, were determined, such as $E(B - V) = 0.08$ given by van den Bergh (1969), 0.11 given by McClure & Racine (1969), and 0.08 given by Frogel, Persson, & Cohen (1980). As Crampton et al. (1985) did, we use the value of 0.10 as the foreground color excess.

The reddening of GCs in M31 has been determined by several ways in previous studies. As is mentioned, Vetešnik (1962a) compiled a comprehensive catalog of 257 GC candidates, and derived color excesses for the candidates that were considered to be most probably the GCs (Vetešnik 1962b). To obtain true colors of the clusters, Vetešnik (1962b) calculated the average true color index of 36 GCs beyond the body of M31, and considered the result, $B - V = 0.83$ mag, as the uniform value of true color for all GCs in M31. Actually, this implicated that these clusters were only affected by the foreground Galactic extinction. Later, many authors used this assumption of a single intrinsic color for all GCs in M31 (Bajaja & Gergely 1977; Iye & Richter 1985).

Using the slope parameter, S , Crampton et al. (1985) calculated intrinsic colors for individual GCs. S , defined by Hartwick (1968), was proved to be a good indicator of intrinsic color and metallicity. From the derived relationship between $(B - V)_0$ and S , Crampton et al. (1985) gave intrinsic colors and color excesses for most candidates in their catalog.

A comprehensive list of colors and metallicities for the M31 GCs was given by Barmby et al. (2000). In order to determine the cluster reddening, they set two reasonable assumptions that both the extinction law and the GC intrinsic color were the same. By using the color-metallicity relationships and the relationships between colors and reddening-free parameters, two basic methods were used independently to obtain the intrinsic colors. Finally, for each GC, the two results were combined by their own weight.

In present paper, we mainly use color excesses given by Barmby et al. (2000) for reddening correction. Since our sample contains a total of 172 GCs, and values of $E(B - V)$ for only 152 of 172 objects were derived by Barmby et al. (2000), there remains 20 objects undetermined. We note that values of S, the slope parameter, for 9 of these 20 GCs were given by Crampton et al. (1985), the intrinsic colors for these 9 GCs can be derived from the equation given by Crampton et al. (1985):

$$(B - V)_0 = 0.066S - 0.17(B - V) + 0.32, \quad (5)$$

where the values of S are taken from Crampton et al. (1985) and values of $B - V$ comes from Barmby et al. (2000). At last there are still 11 GCs whose color excesses are not determined. For these 11 objects, we assume that they are only affected by the foreground Galactic extinction and their color excesses are the foreground color excess, i.e., $E(B - V) = 0.10$. In addition, we adopted the extinction curve presented by Zombeck (1990). An extinction correction $A_\lambda = R_\lambda E(B - V)$ was applied, here R_λ is obtained by interpolating using the data of Zombeck (1990).

5. AGE ESTIMATES

After the photometric measurements are dereddened, intrinsic colors for each GC depend on two parameters, age and metallicity, since we model the stellar populations of the GCs by SSPs. In this section we will determine the ages and best-fitted model of metallicity for our sample GCs simultaneously by the least-square method. The age and best-fitted models of metallicity are found by minimizing the difference between the intrinsic colors of the sample GCs and integrated colors of GSSP:

$$R^2(n, t, Z) = \frac{\sum_{i=3}^{15} [C_{\lambda_i}^{\text{intr}}(n) - C_{\lambda_i}^{\text{ssp}}(t, Z)]^2 / \sigma_i^2}{\sum_{i=3}^{15} 1 / \sigma_i^2}, \quad (6)$$

where $C_{\lambda_i}^{\text{ssp}}(t, Z)$ is the integrated color in the i th filter of a SSP at age t in the model of metallicity Z , and $C_{\lambda_i}^{\text{intr}}(n)$ presents the intrinsic integrated color in the same filter of the n th GC. The differences are weighted by $1/\sigma_i^2$, where the σ_i 's are observational uncertainties of the passbands. The M31 GCs generally have a metal abundance, $[Fe/H]$, lower than 0.0

(Barmby et al. 2000), which corresponds to $Z = 0.0169$ (Leitherer et al. 1996), so we only select the models of three metallicity, 0.0004, 0.004 and 0.02 of GSSP.

Figure 4 shows the fit of the integrated color of a SSP ($Z = 0.0004$, 0.004 and 0.02) with the intrinsic color for 20 GCs selected from the 172 GCs (the first 20 GCs in Table 2). In Figure 4, filled circle represents the intrinsic integrated color of a GC, and the thick line represents the best fit of the integrated color of a SSP of GSSP. From Figure 4, we see that SEDs of GCs are fitted very well by the best-fitted SSP of GSSP model. Table 3 presents ages and the best-fitted models of metallicities for all the 172 GCs. The uncertainties in the age estimates arising from photometric uncertainties are 0.2 or so, i.e, $\text{age} \pm 0.2 \times \text{age}$ [log yr]. In addition, we noted that clusters 127 and 225 have strong emission lines in the filter of BATC09, so we did not use the color of this filter in the process of fitting.

We should emphasize that, in this study, we estimate the ages of our sample clusters by comparing the photometry of each object with models for different values of metallicity as Chandar, Bianchi, & Ford (1999b, 1999c, 2001) did. Recently, using the similar technique, Ma et al. (2002a) estimated ages of 10 halo GCs in M33 with four models of metallicities ($Z = 0.0004$, 0.004, 0.008, and 0.02). Here we use three metallicity models to estimate ages for our sample GCs. In each model, the ages of SSPs are from 0 to 20 Gyrs. We should also emphasize that, for very old globular clusters, the age/metallicity degeneracy becomes pronounced. In this case, we only mean that in some model of metallicity, the intrinsic integrated color of a GC can do the best fit with the integrated color of a SSP at some age.

From Table 3, we see that most GCs are old objects, except clusters 133 and 362. Cluster 133 appears to be very young, and its reddening-corrected SED significantly differs from others'. This case can be explained by the high value of $E(B - V)$. Since $E(B - V)$ of cluster 133 was not given by Barmby et al. (2000), we calculated its value using S (see Sec. 4). According to equation (5), $E(B - V)$ is determined as follows:

$$E(B - V) = 1.17(B - V) - 0.066S - 0.32, \quad (7)$$

where $B - V$ comes from Barmby et al. (2000), and S from Crampton et al. (1985), as has been described in Sec. 4. From equation (7), we can see that a high value of $B - V$ and a

small value of S all lead to high $E(B - V)$. Besides, we should note that the value of $B - V$ of cluster 133 given by Barmby et al. (2000) is 0.93, while the corresponding values given by Battistini et al. (2000) and the BATC photometry are 0.66 and 0.26 respectively. The value of S given by Crampton et al. (1985) is very low, −4, while values of most S are more than 0. Due to these two reasons, or maybe one of the two reasons, cluster 133 appears very young. Another “young” cluster is cluster 362, whose $E(B - V)$ given by Barmby et al. (2000) is 0.42, but the uncertainty of $E(B - V)$ is 0.45. Perhaps due to the big uncertainty of $E(B - V)$, cluster 362 also appears very young. In the next analysis, we do not include these two GCs.

Figure 5 plots histograms of GC ages for three models of different metallicities, $Z = 0.02, 0.004$, and 0.0004 , and for all GCs, except clusters 133 and 362. From this figure, we can see that almost all these GCs have ages more than 10^9 years, and most of them are around 10^{10} years old. In the separated histograms of three models, only a few GCs are included in $Z = 0.02$ model, while most GCs are included in $Z = 0.004$ and $Z = 0.0004$ models. We can also see that ages in $Z = 0.004$ and $Z = 0.0004$ models have apparently different distributions. The peak of age in $Z = 0.004$ model is at about 6 Gyr, while the peak in $Z = 0.0004$ model is about 19 Gyr. This means, in general, GCs in $Z = 0.0004$ model are older than those in $Z = 0.004$ model.

Barmby & Huchra (2000) compared simple stellar population colors of three population synthesis models to the intrinsic colors of Galactic and M31 GCs in $UBVRIJHK$ colors. They found that higher metallicity cluster colors are best fit by the younger models, and lower metallicity cluster colors are best fit by the older models. Our results in this paper are in agreement with Barmby & Huchra (2000).

It is well known that the abundance distributions of GCs in many galaxies are bimodal, including M31 GC system (e.g. Barmby et al. 2000; Perrett et al. 2002). Forbes, Brodie, & Grillmair (1997) found that the metal-rich GCs in elliptical and cD galaxies are closely coupled to their parent galaxies, but the metal-poor GCs are largely independent of the galaxies. They concluded that the metal-poor GCs are formed during the beginning of

galaxy formation, and the metal-rich GCs are formed at a later stage than metal-poor GCs. If so, this may imply that the age distribution of GCs should be bimodal or multi-modal. Due to our incomplete sample, from Figure 5 we can not confirm whether or not the age distribution is bimodal or multi-modal, however, we can say that the age distribution of GCs in M31 is not monomodel.

The presence of groups of clusters in space and in age is interesting. We show the GC age as a function of galactocentric distance R in Figure 6. The galactocentric distance R for M31 GCs is derived using the distance modulus of 24.47 (Holland 1998; Stanek & Garnavich 1998), the inclination angle of 77 degrees (Williams & Hodge 2001), and the position angle of 38 degrees (Williams & Hodge 2001). Figure 6 shows that, there exists a few groups of clusters which are nearby in space and in age. This result tells us that some nearby GCs formed simultaneously. We also plot age versus reddening-corrected apparent magnitude in Figure 7, no trend is obvious.

6. SUMMARY

In the present paper, we for the first time obtained the SEDs for 172 GCs of M31 in 13 intermediate band filters, with the BATC 60/90 cm Schmidt telescope. The main results and conclusions are summarized as follows:

1. Using the images obtained with the BATC Multicolor Sky Survey Telescope, we obtained SEDs for 172 GCs of M31 selected from the Bologna catalog, in 13 intermediate-band filters covering a range of wavelength from 3800 to 10000Å. We also gave identification charts for 219 class A or B GCs of Bologna catalog in our CCD field.
2. Using the relationship between the BATC intermediate-band system and the *UBVRI* broad-band system, we derived the magnitudes in the *B* and *V* bands. The computed *V* and $B - V$ are in agreement with previous measurements.
3. By comparing the photometry of each GC with theoretical stellar population synthesis models, we estimated ages of the sample GCs for different metallicities. The

results show that nearly all the GCs have ages more than 10^9 years, and GCs in the metal-poor model are generally older than ones in the metal-rich model.

We would like to thank the anonymous referee for his/her insightful comments and suggestions that improved this paper. We are grateful to P. Barmby and J. P. Huchra for providing us values of $E(B - V)$ for GCs in M31 that they derived. We would like to thank the Padova group for providing us with a set of theoretical isochrones and SSPs. We are also indebted to G. Bruzual and S. Charlot for sending us their latest calculations of SSPs and for explanations of their code. The work is supported partly by the National Sciences Foundation under the contract No.19833020 and No.19503003. The BATC Survey is supported by the Chinese Academy of Sciences, the Chinese National Natural Science Foundation and the Chinese State Committee of Sciences and Technology. The project is also supported in part by the National Science Foundation (grant INT 93-01805) and by Arizona State University, the University of Arizona and Western Connecticut State University.

REFERENCES

- Ashman, K. M., & Bird, C. M. 1993, AJ, 106, 2281
- Aurière, M., Coupinot, G., & Hecquet, J. 1992, A&A, 256, 95
- Bajaja, E., & Gergely, T. E. 1977, A&A, 61, 229
- Barmby, P., Huchra, J. P., Brodie, J. P., Forbes, D. A., Schroder, L. L., & Grillmair, C. J. 2000, AJ, 119, 727
- Barmby, P., & Huchra, J. P. 2000, ApJ, 531, 29
- Barmby, P., Huchra, J. P., & Brodie, J. P. 2001, AJ, 121, 1482
- Barmby, P., & Huchra, J. P. 2001, AJ, 122, 2458
- Battistini, P., Bònoli, F., Braccesi, A., Federici, L., Fusi Pecci F., Marano, B., & Börngen, F. 1987, A&AS, 67, 447
- Battistini, P., Bònoli, F., Braccesi, A., Fusi Pecci F., Malagnini, M. L., & Marano, B. 1980, A&AS, 42, 357
- Battistini, P., Bònoli, F., Casavecchia, M., Ciotti, L., Federici, L., & Fusi Pecci F. 1993, A&A, 272, 77
- Borges A. C., Idiart T. P., de Freitas Pacheco J. A., & Thevenin F. 1995, AJ, 110, 2408
- Bressan, A., Chiosi, C., & Tantalo, R. 1996, A&A, 311, 425
- Bruzual, A. G., & Charlot, S. 1993, ApJ, 405, 538
- Buzzoni, A. 1997, in IAU Symp. 183, Cosmological Parameters and Evolution of the Universe, ed. K. Sato, 18
- Calzetti, D. 1997, AJ, 113, 162
- Charlot, S., & Bruzual, A. G. 1991, ApJ, 367, 126

- Chiosi, C., Bressan, A., Portinari, L., & Tantalo, R. 1998, A&A, 339, 355
- Crampton, D., Cowley, A. P., Schade, D., & Chayer, P. 1985, ApJ, 288, 494
- de Freitas Pacheco, J. A. 1997, A&A, 319, 394
- Fan, X., et al. 1996, AJ, 112, 628
- Fioc, M., & Rocca-Volmerange, B. 1997, A&A, 326, 950
- Forbes, D. A., Brodie, J. P., & Grillmair, C. J. 1997, AJ, 113, 1652
- Frogel, J. A., Persson, S. E., & Cohen, J. G. 1980, ApJ, 240, 785
- Fusi Pecci F., Cacciari, C., Federici, L., & Pasquali, A. 1993, in: The Globular Cluster-Galaxy Connection, eds. G. H. Smith, J. P. Brodie, Vol. 48, p. 410
- Galadí-Enríquez, D., Trullols, E., & Jordi, C. 2000, A&AS, 146, 169
- Harris, W. E. 1991, ARA&A, 29, 543
- Hartwick, F. D. A. 1968, ApJ, 154, 475
- Hiltner, W. A. 1958, ApJ, 128, 9
- Hiltner, W. A. 1960, ApJ, 131, 163
- Holland, S. 1998, AJ, 115, 1916
- Hubble, E. 1932, ApJ, 76, 44
- Iye, M., & Richter, O. -G. 1985, A&A, 144, 471
- Jablonka, P., Alloin, D., & Bica, E. 1992, A&A, 260, 97
- Jablonka, P., Bica, E., Pelat, D., & Alloin, D. 1996, A&A, 307, 385
- Kong, X., et al. 2000, AJ, 119, 2745
- Kron, G. E., & Mayall, N. U. 1960, AJ, 65, 581

- Landolt, A. U. 1983, AJ, 88, 439
- Landolt, A. U. 1992, AJ, 104, 340
- Leitherer, C., et al. 1996, PASP, 108, 996
- Leitherer, C., et al. 1999, ApJS, 123, 3
- Ma, J., et al. 2001, AJ, 122, 1796
- Ma, J., Zhou, X., Chen, J., Wu, H., Jiang, Z. Xue, S., & Zhu, J. 2002a, A&A, 385, 404
- Ma, J., Zhou, X., Chen, J., Wu, H., Jiang, Z. Xue, S., & Zhu, J. 2002b, AJ, 123, 3141
- Mayall, N. U., & Eggen, O. J. 1953, PASP, 65, 24
- McClure, R. D., & Racine, R. 1969, AJ, 74, 1000
- Mochejska, B. J., Kaluzny, J., Krockenberger, M., Sasselov, D. D., & Stanek, K. Z. 1998, AcA, 48, 455
- Mollà, M., Ferrini, F., & Diaz, A. I. 1997, ApJ, 475, 519
- Origlia, L., Goldader, J. D., Leitherer, C. Schaerer, D., & Oliva, E. 1999, ApJ, 514, 96
- Perrett, K. M., et al. 2002, AJ, 123, 2490
- Racine, R. 1991, AJ, 101, 865
- Reed, L. G., Harris G. L. H., & Harris, W. E. 1992, AJ, 103, 824
- Rich, R. M., Corsi, C. E., Bellazzini, M., Federici, L., Cacciari, C., & Fusi Pecci F. 2001, in: Extragalactic Star Clusters, eds. E. K. Grebel, D. Geisler, D. Minniti, Vol. 207
- Salpeter, E. E. 1955, ApJ, 121, 161
- Sargent, W. L. W., Kowal, C. T., Hartwick, F. D. A., & van den Bergh, S. 1977, AJ, 82, 947
- Schaerer, D., & de Koter, A. 1997, A&A, 322, 598
- Schaerer, D., & Vacca, W. D. 1998, ApJ, 497, 618

- Searle, L., Sargent, W. L. W., & Bagnuolo, W. G. 1973, ApJ, 179, 427
- Seyfert, C. K., & Nassau, J. J. 1945, ApJ, 102, 377
- Stanek, K. Z., & Garnavich, P. M. 1998, ApJ, 503, 131
- Stetson, P. B. 1987, PASP, 99, 191
- Stetson, P. B. 1990, PASP, 102, 932
- Tinsley, B. M. 1972, A&A, 20, 383
- van den Bergh, S. 1969, ApJS, 19, 145
- Vazdekis, A., Peletier, R. F., Beckman, J. E., & Casuso, E. 1997, ApJS, 111, 203
- Vetešnik, M. 1962a, BAC, 13, no. 5, p. 182
- Vetešnik, M. 1962b, BAC, 13, no. 6, p. 218
- Williams, B. F., & Hodge, P. W. 2001, ApJ, 559, 851
- Yan, H., et al. 2000, PASP, 112, 691
- Zheng, Z., et al. 1999, AJ, 117, 2757
- Zhou, X., Jiang, Z., Xue, S., Wu, H., Ma, J., & Chen, J. 2001, CJAA, 1, 372
- Zhou, X., et al. 2002, A&A, in press
- Zombeck, M. V. 1990, Handbook of Space Astronomy and Astrophysics (2nd. ed; Cambridge: Cambridge Univ. Press) p. 104

Table 2: SEDs of 172 GCs in M31

No.	03	04	05	06	07	08	09	10	11	12	13	14	15
(1)	(2)	(3)	(4)	(5)	(6)	(7)	(8)	(9)	(10)	(11)	(12)	(13)	(14)
326	16.18	16.16	16.01	16.00	15.78	15.81	15.77	15.69	15.64	15.51	15.47	15.43	15.44
	0.175	0.173	0.185	0.188	0.186	0.197	0.198	0.202	0.206	0.211	0.220	0.212	0.219
328	17.43	17.14	16.92	16.84	16.50	16.49	16.42	16.31	16.21	16.03	15.96	15.96	16.01
	0.106	0.162	0.163	0.162	0.153	0.159	0.159	0.158	0.165	0.159	0.163	0.161	0.177
332	19.27	18.90	18.74	18.91	18.59	18.58	18.51	18.68	18.22	17.96	17.67	18.16	17.67
	0.250	0.225	0.262	0.321	0.337	0.356	0.375	0.488	0.369	0.340	0.301	0.463	0.311
333	19.35	18.90	18.74	18.48	18.13	18.11	17.86	17.82	17.52	17.50	17.49	17.10	17.24
	0.300	0.245	0.282	0.238	0.239	0.250	0.221	0.241	0.211	0.240	0.279	0.185	0.221
9	17.82	17.38	17.12	17.04	16.69	16.65	16.55	16.50	16.38	16.24	16.35	16.24	16.25
	0.028	0.022	0.020	0.021	0.021	0.021	0.022	0.025	0.028	0.025	0.042	0.028	0.040
11	17.61	17.17	16.87	16.76	16.41	16.36	16.24	16.16	16.04	15.93	15.97	15.90	15.90
	0.038	0.031	0.031	0.030	0.031	0.030	0.030	0.032	0.035	0.036	0.042	0.041	0.043
14	20.15	19.23	18.51	18.14	17.80	17.64	17.33	17.28	17.19	17.07	16.80	16.70	16.52
	0.103	0.045	0.027	0.024	0.024	0.019	0.022	0.013	0.018	0.008	0.038	0.009	0.038
15	19.20	18.59	18.25	17.93	17.50	17.36	17.02	16.83	16.60	16.42	16.45	16.05	16.01
	0.108	0.063	0.059	0.046	0.039	0.036	0.027	0.026	0.023	0.020	0.036	0.019	0.029
17	17.16	16.72	16.36	16.10	15.69	15.59	15.32	15.18	15.04	14.90	14.86	14.66	14.59
	0.012	0.006	0.005	0.005	0.004	0.004	0.004	0.004	0.004	0.003	0.007	0.004	0.008
21	18.73	18.25	17.93	17.69	17.31	17.21	16.92	16.76	16.59	16.43	16.44	16.13	16.10
	0.048	0.037	0.031	0.031	0.030	0.027	0.025	0.023	0.024	0.021	0.030	0.023	0.034
23	15.49	14.98	14.63	14.35	13.95	13.85	13.58	13.44	13.29	13.17	13.11	12.90	12.85
	0.003	0.002	0.002	0.002	0.002	0.001	0.001	0.001	0.001	0.001	0.002	0.002	0.002
25	17.69	17.36	17.10	16.87	16.56	16.49	16.24	16.16	16.09	16.02	16.01	15.86	15.87
	0.015	0.012	0.011	0.012	0.012	0.010	0.012	0.014	0.017	0.014	0.025	0.024	0.031
27	16.41	16.12	15.90	15.73	15.45	15.39	15.19	15.09	15.05	15.00	14.99	14.83	14.83
	0.007	0.007	0.006	0.006	0.006	0.006	0.005	0.005	0.005	0.005	0.008	0.007	0.010
28	17.63	17.37	17.12	16.97	16.72	16.67	16.43	16.33	16.27	16.21	16.20	16.01	16.00
	0.013	0.012	0.011	0.011	0.012	0.010	0.012	0.013	0.017	0.014	0.026	0.024	0.032

Table 2: Continued

No.	03	04	05	06	07	08	09	10	11	12	13	14	15	
	(1)	(2)	(3)	(4)	(5)	(6)	(7)	(8)	(9)	(10)	(11)	(12)	(13)	(14)
33	19.03	18.80	18.45	18.18	17.89	17.70	17.52	17.35	17.45	17.35	17.29	17.16	17.05	
	0.071	0.074	0.067	0.056	0.056	0.045	0.044	0.043	0.052	0.050	0.064	0.065	0.075	
34	16.46	16.03	15.77	15.59	15.28	15.23	14.98	14.87	14.76	14.71	14.74	14.49	14.50	
	0.006	0.004	0.003	0.003	0.004	0.004	0.004	0.004	0.004	0.004	0.008	0.005	0.007	
36	18.38	17.96	17.64	17.45	17.09	16.97	16.79	16.70	16.53	16.45	16.34	16.20	16.20	
	0.022	0.014	0.010	0.011	0.013	0.010	0.012	0.012	0.016	0.012	0.030	0.021	0.030	
37	19.28	18.47	17.81	17.23	16.40	16.14	15.54	15.25	14.89	14.61	14.32	13.95	13.78	
	0.061	0.032	0.021	0.016	0.012	0.009	0.007	0.006	0.006	0.004	0.007	0.004	0.005	
38	17.35	17.04	16.74	16.56	16.22	16.13	15.94	15.82	15.74	15.65	15.56	15.43	15.38	
	0.014	0.011	0.009	0.009	0.009	0.009	0.009	0.009	0.010	0.011	0.017	0.014	0.018	
39	17.44	16.91	16.51	16.23	15.75	15.63	15.34	15.19	15.00	14.88	14.71	14.54	14.49	
	0.016	0.010	0.009	0.008	0.007	0.006	0.005	0.005	0.006	0.005	0.009	0.006	0.008	
41	18.82	18.26	17.96	17.88	17.43	17.35	17.19	17.05	16.95	16.86	16.73	16.73	16.66	
	0.131	0.106	0.107	0.108	0.098	0.097	0.094	0.092	0.097	0.100	0.111	0.101	0.101	
42	18.03	17.44	16.93	16.47	15.89	15.71	15.32	15.13	14.94	14.76	14.63	14.40	14.34	
	0.071	0.062	0.056	0.044	0.039	0.036	0.030	0.028	0.027	0.026	0.027	0.022	0.021	
44	17.92	17.44	17.07	16.85	16.45	16.34	16.12	15.97	15.84	15.72	15.61	15.45	15.44	
	0.022	0.013	0.011	0.010	0.010	0.008	0.009	0.009	0.010	0.008	0.016	0.012	0.017	
48	17.60	17.14	16.82	16.63	16.28	16.21	15.98	15.85	15.72	15.61	15.55	15.32	15.31	
	0.023	0.021	0.019	0.018	0.019	0.018	0.018	0.019	0.020	0.021	0.025	0.024	0.026	
51	17.44	16.93	16.54	16.29	15.87	15.77	15.52	15.38	15.22	15.09	14.99	14.82	14.79	
	0.011	0.007	0.006	0.005	0.005	0.004	0.004	0.004	0.005	0.004	0.007	0.007	0.009	
53	18.91	18.47	18.18	18.11	17.80	17.78	17.69	17.63	17.58	17.49	17.50	17.39	17.28	
	0.053	0.045	0.038	0.042	0.045	0.042	0.048	0.051	0.056	0.065	0.078	0.086	0.090	
54	19.07	18.68	18.34	18.18	17.84	17.84	17.59	17.43	17.20	17.17	17.15	16.74	16.65	
	0.066	0.065	0.053	0.055	0.052	0.049	0.051	0.051	0.054	0.054	0.060	0.058	0.064	
56	18.38	17.84	17.55	17.38	17.01	16.97	16.69	16.57	16.37	16.32	16.33	16.00	15.89	
	0.032	0.024	0.018	0.018	0.020	0.018	0.017	0.019	0.018	0.020	0.026	0.022	0.026	

Table 2: Continued

No.	03	04	05	06	07	08	09	10	11	12	13	14	15	
	(1)	(2)	(3)	(4)	(5)	(6)	(7)	(8)	(9)	(10)	(11)	(12)	(13)	(14)
63	17.06	16.51	16.08	15.85	15.36	15.26	14.99	14.84	14.64	14.55	14.46	14.19	14.16	
	0.011	0.007	0.005	0.005	0.004	0.004	0.004	0.004	0.004	0.004	0.006	0.004	0.006	
64	17.01	16.72	16.45	16.29	16.05	15.99	15.82	15.73	15.62	15.56	15.49	15.39	15.44	
	0.019	0.021	0.021	0.020	0.022	0.021	0.021	0.023	0.025	0.028	0.031	0.031	0.036	
67	17.90	17.60	17.37	17.24	17.02	16.99	16.81	16.73	16.69	16.69	16.51	16.59	16.71	
	0.020	0.021	0.021	0.022	0.026	0.026	0.032	0.031	0.042	0.043	0.052	0.057	0.078	
68	17.70	17.11	16.76	16.49	16.07	15.96	15.64	15.51	15.34	15.29	15.17	14.91	14.90	
	0.020	0.014	0.010	0.009	0.008	0.007	0.007	0.006	0.007	0.006	0.011	0.007	0.012	
69	18.54	18.42	18.18	18.18	18.02	18.02	17.86	17.88	17.90	17.87	17.82	17.88	17.73	
	0.034	0.034	0.032	0.037	0.048	0.044	0.051	0.053	0.065	0.059	0.134	0.106	0.138	
70	17.45	17.21	16.98	16.83	16.59	16.55	16.39	16.32	16.28	16.21	16.18	16.07	16.05	
	0.017	0.017	0.016	0.017	0.018	0.015	0.020	0.020	0.023	0.023	0.033	0.033	0.045	
71	19.49	18.87	18.49	18.19	17.82	17.65	17.36	17.16	17.01	16.80	16.87	16.82	16.98	
	0.160	0.130	0.122	0.113	0.118	0.107	0.108	0.097	0.104	0.100	0.134	0.144	0.184	
72	18.19	17.99	17.66	17.39	16.81	16.61	16.40	16.13	15.88	15.66	15.38	15.35	15.22	
	0.033	0.040	0.042	0.036	0.032	0.026	0.027	0.025	0.025	0.022	0.026	0.026	0.023	
73	17.00	16.51	16.23	16.07	15.76	15.72	15.51	15.40	15.27	15.26	15.16	15.00	15.00	
	0.018	0.013	0.013	0.011	0.012	0.010	0.010	0.010	0.012	0.011	0.019	0.013	0.018	
75	18.29	17.88	17.56	17.39	17.03	16.95	16.76	16.65	16.55	16.45	16.29	16.24	16.27	
	0.034	0.031	0.029	0.028	0.030	0.029	0.032	0.032	0.037	0.039	0.045	0.050	0.058	
76	17.63	17.30	17.01	16.82	16.57	16.51	16.31	16.20	16.15	16.10	16.03	15.91	15.98	
	0.019	0.016	0.016	0.016	0.017	0.016	0.019	0.019	0.024	0.024	0.035	0.032	0.042	
77	19.12	18.36	17.94	17.56	17.19	17.04	16.77	16.61	16.45	16.34	16.29	16.08	16.05	
	0.144	0.101	0.087	0.065	0.059	0.047	0.041	0.037	0.038	0.034	0.046	0.039	0.047	
78	20.01	18.88	18.39	17.99	17.37	17.28	16.86	16.69	16.46	16.28	16.09	15.91	15.87	
	0.521	0.295	0.262	0.214	0.177	0.178	0.146	0.141	0.133	0.129	0.121	0.113	0.110	
79	19.56	18.75	18.27	17.91	17.54	17.33	17.04	16.89	16.71	16.52	16.35	16.06	16.03	
	0.091	0.054	0.039	0.032	0.030	0.025	0.023	0.023	0.021	0.020	0.025	0.021	0.030	

Table 2: Continued

No.	03	04	05	06	07	08	09	10	11	12	13	14	15	
	(1)	(2)	(3)	(4)	(5)	(6)	(7)	(8)	(9)	(10)	(11)	(12)	(13)	(14)
88	16.64	16.26	15.86	15.60	15.16	15.05	14.80	14.66	14.52	14.36	14.26	14.09	14.06	
	0.008	0.006	0.004	0.004	0.004	0.003	0.003	0.003	0.003	0.003	0.005	0.004	0.005	
90	19.19	18.53	18.33	18.25	18.03	18.05	17.81	17.80	17.70	17.87	17.83	17.44	17.51	
	0.133	0.091	0.103	0.106	0.102	0.106	0.102	0.113	0.126	0.169	0.193	0.147	0.183	
91	17.82	17.61	17.49	17.47	17.27	17.28	17.25	17.18	17.21	17.15	17.04	17.06	17.23	
	0.039	0.041	0.049	0.053	0.057	0.061	0.069	0.073	0.090	0.094	0.111	0.129	0.166	
92	17.76	17.44	17.17	17.01	16.74	16.68	16.51	16.40	16.37	16.29	16.22	16.14	16.14	
	0.034	0.035	0.034	0.035	0.038	0.037	0.039	0.040	0.048	0.050	0.057	0.065	0.072	
93	17.89	17.51	17.12	16.92	16.59	16.51	16.30	16.14	15.96	15.79	15.65	15.52	15.50	
	0.047	0.045	0.042	0.039	0.040	0.039	0.038	0.036	0.034	0.034	0.035	0.035	0.038	
94	16.62	16.14	15.86	15.69	15.37	15.31	15.06	14.95	14.83	14.79	14.77	14.52	14.51	
	0.008	0.005	0.005	0.004	0.004	0.003	0.004	0.004	0.004	0.004	0.006	0.005	0.008	
96	17.78	17.19	16.78	16.59	16.15	16.00	15.77	15.62	15.44	15.30	15.11	15.04	15.00	
	0.126	0.111	0.108	0.101	0.094	0.088	0.082	0.080	0.079	0.081	0.077	0.074	0.072	
97	18.04	17.60	17.19	16.98	16.56	16.47	16.28	16.14	16.02	15.93	15.78	15.67	15.63	
	0.027	0.025	0.022	0.021	0.020	0.019	0.020	0.019	0.021	0.021	0.025	0.025	0.030	
98	17.17	16.76	16.49	16.32	16.03	15.97	15.76	15.68	15.61	15.56	15.48	15.35	15.40	
	0.011	0.007	0.007	0.007	0.007	0.006	0.007	0.007	0.008	0.007	0.014	0.011	0.017	
99	17.57	17.24	16.93	16.83	16.53	16.50	16.39	16.23	16.16	16.09	15.97	15.81	15.82	
	0.047	0.047	0.054	0.049	0.055	0.056	0.058	0.058	0.066	0.071	0.078	0.074	0.083	
101	17.73	17.38	17.11	16.97	16.70	16.65	16.44	16.36	16.19	16.09	16.00	15.85	15.81	
	0.036	0.038	0.039	0.040	0.044	0.044	0.040	0.044	0.045	0.050	0.055	0.049	0.056	
103	16.36	15.81	15.44	15.27	14.93	14.84	14.61	14.48	14.31	14.23	14.07	13.93	13.92	
	0.077	0.068	0.066	0.061	0.061	0.060	0.054	0.054	0.054	0.059	0.058	0.052	0.054	
102	17.21	16.94	16.72	16.66	16.41	16.38	16.33	16.24	16.22	16.13	16.15	16.08	16.07	
	0.010	0.008	0.007	0.008	0.010	0.009	0.011	0.012	0.015	0.015	0.026	0.023	0.032	
104	17.65	17.32	17.10	17.02	16.75	16.68	16.58	16.55	16.51	16.38	16.11	16.69	16.82	
	0.262	0.279	0.322	0.321	0.362	0.363	0.373	0.407	0.475	0.485	0.433	0.769	0.911	

Table 2: Continued

No.	03	04	05	06	07	08	09	10	11	12	13	14	15	
	(1)	(2)	(3)	(4)	(5)	(6)	(7)	(8)	(9)	(10)	(11)	(12)	(13)	(14)
109	17.46	17.00	16.66	16.51	16.15	16.05	15.88	15.74	15.55	15.50	15.30	15.14	15.09	
	0.046	0.049	0.044	0.046	0.052	0.049	0.049	0.050	0.053	0.057	0.055	0.053	0.056	
111	17.51	17.23	17.00	16.84	16.60	16.57	16.36	16.28	16.25	16.22	16.15	16.07	16.06	
	0.017	0.014	0.012	0.011	0.013	0.012	0.012	0.013	0.016	0.014	0.026	0.024	0.031	
110	16.08	15.69	15.41	15.25	14.97	14.92	14.71	14.60	14.50	14.44	14.36	14.23	14.23	
	0.005	0.004	0.003	0.004	0.004	0.003	0.004	0.004	0.004	0.004	0.007	0.006	0.008	
112	17.45	16.84	16.47	16.34	15.98	15.87	15.63	15.49	15.27	15.21	15.02	14.90	14.88	
	0.291	0.241	0.236	0.227	0.230	0.223	0.201	0.200	0.192	0.217	0.209	0.192	0.196	
114	17.40	17.16	16.90	16.75	16.54	16.48	16.35	16.23	16.15	16.06	15.90	15.65	15.59	
	0.113	0.136	0.152	0.147	0.175	0.177	0.188	0.188	0.213	0.239	0.235	0.204	0.203	
117	16.98	16.70	16.50	16.35	16.08	16.10	15.87	15.84	15.82	15.74	15.72	15.59	15.65	
	0.012	0.011	0.011	0.014	0.014	0.013	0.012	0.011	0.014	0.017	0.021	0.020	0.033	
115	16.91	16.34	15.95	15.84	15.45	15.36	15.17	15.03	14.86	14.77	14.60	14.47	14.40	
	0.150	0.132	0.131	0.131	0.133	0.132	0.127	0.130	0.133	0.143	0.145	0.131	0.130	
116	18.45	17.81	17.36	17.00	16.44	16.28	15.95	15.77	15.53	15.36	15.18	14.95	14.86	
	0.026	0.016	0.013	0.011	0.011	0.008	0.007	0.007	0.008	0.007	0.011	0.008	0.010	
118	16.75	16.39	16.02	15.92	15.58	15.53	15.37	15.31	15.18	15.08	14.98	14.89	14.95	
	0.224	0.240	0.244	0.248	0.263	0.272	0.274	0.296	0.316	0.334	0.363	0.348	0.390	
122	19.53	18.81	18.32	17.96	17.35	17.16	16.83	16.64	16.42	16.22	16.12	15.82	15.72	
	0.056	0.038	0.025	0.022	0.019	0.015	0.014	0.013	0.014	0.013	0.021	0.016	0.020	
123	18.29	17.85	17.50	17.36	17.09	17.02	16.79	16.69	16.59	16.51	16.37	16.34	16.33	
	0.119	0.123	0.121	0.119	0.135	0.133	0.126	0.131	0.144	0.164	0.169	0.167	0.178	
125	17.18	16.91	16.68	16.54	16.32	16.30	16.13	16.03	16.01	15.98	15.86	15.81	15.89	
	0.011	0.012	0.013	0.013	0.015	0.015	0.017	0.018	0.022	0.022	0.030	0.025	0.036	
126	17.63	17.27	17.04	16.82	16.52	16.48	16.33	16.22	16.07	16.03	15.80	15.93	15.83	
	0.194	0.209	0.239	0.215	0.238	0.244	0.249	0.258	0.271	0.312	0.292	0.348	0.329	
127	15.08	14.65	14.31	14.17	13.84	13.77	12.33	13.48	13.36	13.27	13.11	13.09	13.07	
	0.092	0.093	0.096	0.093	0.100	0.101	0.031	0.102	0.111	0.118	0.122	0.125	0.129	

Table 2: Continued

No.	03	04	05	06	07	08	09	10	11	12	13	14	15	
	(1)	(2)	(3)	(4)	(5)	(6)	(7)	(8)	(9)	(10)	(11)	(12)	(13)	(14)
133	17.47	17.47	17.33	17.30	17.23	17.21	17.11	16.97	16.74	16.71	16.60	16.57	16.59	
	0.100	0.123	0.141	0.142	0.167	0.169	0.165	0.159	0.138	0.152	0.166	0.153	0.163	
134	17.14	16.71	16.49	16.29	15.98	15.90	15.74	15.60	15.51	15.42	15.23	15.18	15.32	
	0.187	0.190	0.219	0.200	0.220	0.219	0.221	0.221	0.247	0.270	0.265	0.261	0.310	
135	16.95	16.60	16.26	16.08	15.73	15.64	15.46	15.35	15.24	15.15	15.05	14.94	14.91	
	0.008	0.007	0.005	0.006	0.006	0.005	0.006	0.006	0.007	0.007	0.010	0.009	0.012	
136	17.20	16.83	16.51	16.44	16.27	16.24	16.11	16.06	16.04	15.92	15.69	15.76	15.73	
	0.102	0.108	0.113	0.119	0.147	0.153	0.156	0.173	0.208	0.221	0.206	0.235	0.240	
137	19.22	18.68	18.25	17.93	17.46	17.33	17.05	16.87	16.72	16.56	16.44	16.21	16.15	
	0.063	0.049	0.043	0.033	0.032	0.030	0.024	0.024	0.026	0.026	0.036	0.025	0.033	
138	16.93	16.46	16.11	16.00	15.68	15.62	15.50	15.34	15.17	15.14	14.99	14.94	14.99	
	0.123	0.122	0.126	0.124	0.132	0.133	0.140	0.136	0.139	0.161	0.165	0.164	0.180	
141	17.93	17.56	17.20	17.00	16.63	16.52	16.33	16.20	16.09	16.00	15.88	15.73	15.70	
	0.019	0.014	0.014	0.012	0.014	0.013	0.012	0.013	0.014	0.014	0.022	0.018	0.022	
143	17.11	16.55	16.19	16.08	15.74	15.66	15.48	15.34	15.23	15.14	15.00	14.88	14.86	
	0.070	0.061	0.064	0.063	0.071	0.071	0.067	0.068	0.076	0.086	0.089	0.081	0.085	
144	17.41	16.99	16.60	16.44	16.15	16.13	15.94	15.82	15.67	15.58	15.42	15.37	15.35	
	0.159	0.166	0.170	0.171	0.196	0.208	0.210	0.218	0.234	0.257	0.259	0.264	0.271	
145	18.79	18.33	17.99	17.78	17.59	17.53	17.47	17.24	17.21	17.23	17.14	16.88	17.19	
	0.188	0.178	0.179	0.166	0.199	0.195	0.218	0.200	0.237	0.294	0.307	0.255	0.350	
146	17.89	17.41	17.11	16.98	16.70	16.65	16.50	16.32	16.18	16.08	15.95	15.91	15.87	
	0.187	0.185	0.198	0.196	0.222	0.226	0.230	0.222	0.237	0.259	0.270	0.263	0.264	
148	16.63	16.31	15.98	15.86	15.51	15.47	15.32	15.19	15.12	15.01	14.89	14.84	14.85	
	0.053	0.059	0.060	0.059	0.062	0.065	0.063	0.067	0.076	0.081	0.085	0.085	0.091	
149	18.07	17.69	17.31	17.11	16.70	16.59	16.40	16.27	16.17	16.05	15.96	15.78	15.79	
	0.025	0.018	0.015	0.014	0.013	0.011	0.011	0.012	0.014	0.014	0.022	0.018	0.024	
150	17.45	17.00	16.65	16.50	16.19	16.13	15.97	15.81	15.63	15.54	15.36	15.19	15.22	
	0.070	0.062	0.061	0.057	0.061	0.060	0.058	0.058	0.060	0.066	0.067	0.058	0.062	

Table 2: Continued

No.	03	04	05	06	07	08	09	10	11	12	13	14	15	
	(1)	(2)	(3)	(4)	(5)	(6)	(7)	(8)	(9)	(10)	(11)	(12)	(13)	(14)
155	19.00	18.53	18.22	18.00	17.70	17.65	17.40	17.27	17.12	17.08	17.01	16.69	16.67	
	0.049	0.034	0.025	0.023	0.025	0.019	0.023	0.022	0.024	0.023	0.042	0.027	0.055	
157	18.23	17.98	17.74	17.60	17.45	17.40	17.28	17.21	17.28	17.16	17.04	17.01	17.08	
	0.054	0.056	0.060	0.058	0.075	0.068	0.074	0.078	0.108	0.105	0.118	0.105	0.130	
158	15.59	15.19	14.90	14.71	14.44	14.39	14.19	14.08	14.02	13.95	13.84	13.74	13.75	
	0.004	0.003	0.002	0.002	0.002	0.002	0.002	0.002	0.002	0.002	0.004	0.003	0.005	
159	18.12	17.75	17.36	17.23	16.82	16.72	16.49	16.35	16.19	16.01	15.86	15.77	15.77	
	0.037	0.032	0.026	0.025	0.021	0.019	0.020	0.020	0.021	0.019	0.023	0.044	0.050	
160	18.48	18.25	18.09	17.94	17.80	17.62	17.68	17.51	17.59	17.62	17.39	17.28	17.44	
	0.027	0.026	0.027	0.034	0.046	0.029	0.040	0.032	0.044	0.058	0.061	0.056	0.122	
161	17.06	16.74	16.44	16.31	16.05	16.00	15.84	15.75	15.69	15.60	15.50	15.46	15.51	
	0.022	0.022	0.022	0.021	0.023	0.023	0.022	0.024	0.027	0.028	0.032	0.031	0.038	
162	18.52	18.04	17.71	17.55	17.18	17.12	16.85	16.73	16.54	16.39	16.32	15.99	15.97	
	0.055	0.051	0.047	0.047	0.049	0.047	0.044	0.047	0.048	0.052	0.058	0.047	0.054	
163	16.23	15.67	15.30	15.15	14.77	14.69	14.48	14.36	14.18	14.10	14.00	13.80	13.77	
	0.006	0.004	0.004	0.004	0.004	0.004	0.004	0.004	0.004	0.004	0.005	0.005	0.006	
164	18.85	18.31	17.99	17.86	17.46	17.45	17.38	17.08	17.00	16.86	16.85	16.59	16.60	
	0.069	0.044	0.042	0.043	0.049	0.050	0.045	0.048	0.054	0.068	0.082	0.068	0.080	
165	17.04	16.83	16.58	16.47	16.24	16.21	16.08	15.99	15.97	15.86	15.75	15.72	15.74	
	0.014	0.016	0.017	0.016	0.019	0.020	0.021	0.022	0.025	0.026	0.029	0.029	0.039	
166	17.31	17.10	16.84	16.75	16.60	16.61	16.49	16.45	16.43	16.43	16.41	16.40	16.50	
	0.028	0.030	0.030	0.030	0.037	0.039	0.040	0.044	0.057	0.061	0.071	0.078	0.102	
167	18.45	17.99	17.64	17.46	17.13	17.07	16.85	16.75	16.63	16.50	16.44	16.31	16.20	
	0.058	0.058	0.056	0.053	0.060	0.058	0.059	0.061	0.066	0.072	0.079	0.075	0.078	
169	18.48	17.82	17.31	17.23	16.86	16.78	16.55	16.41	16.25	16.10	15.97	15.88	15.82	
	0.063	0.049	0.045	0.047	0.051	0.050	0.050	0.050	0.055	0.057	0.062	0.058	0.061	
171	16.38	15.85	15.49	15.34	15.01	14.95	14.74	14.63	14.48	14.39	14.26	14.16	14.15	
	0.010	0.009	0.008	0.008	0.009	0.009	0.009	0.009	0.010	0.011	0.012	0.011	0.012	

Table 2: Continued

No.	03	04	05	06	07	08	09	10	11	12	13	14	15	
	(1)	(2)	(3)	(4)	(5)	(6)	(7)	(8)	(9)	(10)	(11)	(12)	(13)	(14)
178	15.82	15.52	15.21	15.09	14.82	14.77	14.63	14.53	14.49	14.35	14.26	14.24	14.22	
	0.006	0.005	0.005	0.005	0.005	0.005	0.005	0.006	0.007	0.007	0.009	0.009	0.011	
179	16.23	15.87	15.55	15.42	15.14	15.09	14.95	14.83	14.75	14.65	14.56	14.50	14.53	
	0.014	0.013	0.014	0.013	0.014	0.014	0.015	0.015	0.017	0.018	0.019	0.019	0.022	
180	16.99	16.59	16.28	16.10	15.81	15.76	15.55	15.46	15.39	15.31	15.21	15.13	15.14	
	0.008	0.006	0.005	0.005	0.006	0.004	0.005	0.005	0.007	0.007	0.012	0.010	0.015	
181	17.79	17.40	17.06	16.96	16.58	16.54	16.34	16.28	16.15	16.03	15.93	15.84	15.81	
	0.038	0.030	0.026	0.028	0.026	0.025	0.022	0.026	0.030	0.028	0.035	0.033	0.039	
182	16.43	16.05	15.73	15.50	15.18	15.12	14.88	14.76	14.67	14.58	14.45	14.33	14.29	
	0.006	0.004	0.004	0.004	0.004	0.004	0.004	0.004	0.005	0.005	0.007	0.006	0.008	
183	17.06	16.57	16.27	16.08	15.78	15.72	15.49	15.36	15.27	15.19	15.12	14.95	14.96	
	0.007	0.004	0.003	0.004	0.004	0.004	0.004	0.004	0.004	0.003	0.009	0.005	0.010	
185	16.56	16.11	15.79	15.62	15.32	15.27	15.07	14.96	14.85	14.73	14.64	14.57	14.56	
	0.007	0.006	0.005	0.005	0.006	0.006	0.006	0.007	0.008	0.008	0.009	0.009	0.012	
184	18.66	18.06	17.56	17.47	17.01	16.92	16.69	16.62	16.35	16.21	16.17	15.99	15.93	
	0.051	0.036	0.029	0.028	0.024	0.023	0.021	0.024	0.023	0.023	0.034	0.029	0.033	
186	19.82	18.84	18.52	18.34	17.99	17.79	17.50	17.45	17.07	17.01	16.99	16.59	16.49	
	0.109	0.058	0.050	0.045	0.048	0.036	0.035	0.040	0.034	0.038	0.052	0.038	0.047	
187	18.25	17.98	17.41	17.29	16.93	16.83	16.53	16.46	16.42	16.23	16.13	16.03	16.01	
	0.055	0.049	0.043	0.036	0.035	0.031	0.027	0.028	0.031	0.032	0.048	0.040	0.047	
188	17.71	17.58	17.39	17.30	17.01	16.96	16.78	16.67	16.56	16.42	16.31	16.18	16.15	
	0.080	0.081	0.089	0.082	0.075	0.075	0.062	0.063	0.058	0.055	0.050	0.051	0.060	
189	18.41	17.80	17.39	17.21	16.77	16.69	16.51	16.37	16.17	16.06	16.05	15.80	15.75	
	0.031	0.020	0.016	0.015	0.017	0.015	0.016	0.017	0.018	0.020	0.022	0.021	0.025	
190	17.78	17.40	17.08	16.93	16.60	16.54	16.37	16.25	16.12	16.02	16.01	15.88	15.82	
	0.016	0.012	0.010	0.009	0.014	0.012	0.013	0.014	0.016	0.016	0.022	0.025	0.030	
192	18.33	18.20	18.08	18.02	17.89	17.96	18.04	17.99	17.99	17.84	18.11	18.23	18.20	
	0.038	0.033	0.037	0.038	0.049	0.052	0.066	0.073	0.084	0.091	0.167	0.182	0.212	

Table 2: Continued

No.	03	04	05	06	07	08	09	10	11	12	13	14	15	
	(1)	(2)	(3)	(4)	(5)	(6)	(7)	(8)	(9)	(10)	(11)	(12)	(13)	(14)
200	19.60	19.20	18.87	18.64	18.22	18.09	17.88	17.77	17.60	17.47	17.23	17.36	17.26	
	0.217	0.186	0.170	0.139	0.124	0.110	0.097	0.098	0.101	0.096	0.093	0.130	0.145	
201	16.85	16.56	16.28	16.14	15.87	15.82	15.64	15.55	15.46	15.37	15.14	15.25	15.25	
	0.009	0.008	0.007	0.008	0.008	0.007	0.008	0.010	0.010	0.011	0.013	0.012	0.018	
203	17.67	17.25	16.90	16.76	16.45	16.36	16.18	16.06	15.94	15.85	15.76	15.74	15.70	
	0.019	0.015	0.013	0.013	0.012	0.011	0.012	0.011	0.015	0.012	0.021	0.019	0.024	
204	16.66	16.23	15.92	15.77	15.45	15.39	15.21	15.17	14.98	14.86	14.82	14.73	14.70	
	0.007	0.005	0.004	0.004	0.005	0.004	0.005	0.006	0.007	0.005	0.009	0.007	0.011	
205	16.32	15.94	15.67	15.52	15.23	15.24	15.01	14.90	14.78	14.69	14.63	14.53	14.52	
	0.007	0.005	0.005	0.005	0.005	0.005	0.006	0.005	0.006	0.006	0.009	0.008	0.011	
206	15.92	15.54	15.25	15.13	14.82	14.87	14.86	14.50	14.42	14.32	14.29	14.20	14.20	
	0.005	0.004	0.004	0.003	0.004	0.004	0.005	0.004	0.005	0.004	0.007	0.007	0.008	
208	18.82	18.33	18.02	17.82	17.51	17.43	17.20	17.11	16.94	16.79	16.78	16.61	16.72	
	0.038	0.030	0.026	0.025	0.030	0.025	0.028	0.030	0.032	0.027	0.048	0.039	0.067	
209	17.48	17.11	16.78	16.68	16.43	16.32	16.15	16.08	15.97	15.88	15.93	15.80	15.78	
	0.012	0.009	0.011	0.010	0.013	0.011	0.013	0.014	0.017	0.017	0.029	0.023	0.033	
210	17.92	17.92	17.66	17.58	17.37	17.33	17.21	17.08	16.99	16.94	16.83	16.78	16.87	
	0.022	0.023	0.020	0.022	0.023	0.022	0.028	0.027	0.033	0.030	0.048	0.041	0.067	
211	17.30	17.06	16.79	16.67	16.39	16.38	16.23	16.13	16.06	15.95	15.89	15.86	15.87	
	0.015	0.012	0.011	0.011	0.012	0.011	0.013	0.013	0.016	0.015	0.024	0.018	0.031	
213	17.92	17.42	17.13	16.94	16.79	16.51	16.40	16.31	16.08	15.93	15.99	15.84	15.77	
	0.027	0.022	0.020	0.017	0.023	0.017	0.019	0.018	0.019	0.018	0.026	0.024	0.028	
214	18.32	18.11	17.84	17.79	17.55	17.44	17.26	17.25	17.05	17.00	16.88	16.93	17.06	
	0.037	0.037	0.038	0.038	0.043	0.038	0.037	0.043	0.048	0.047	0.064	0.067	0.097	
215	18.26	17.80	17.44	17.28	16.95	16.90	16.69	16.59	16.42	16.32	16.29	16.12	16.07	
	0.024	0.023	0.021	0.022	0.022	0.022	0.018	0.023	0.023	0.023	0.032	0.030	0.040	
216	17.53	17.39	17.29	17.27	17.14	17.14	17.14	17.11	17.03	17.02	17.18	17.02	16.91	
	0.023	0.024	0.027	0.027	0.035	0.038	0.042	0.045	0.056	0.058	0.086	0.078	0.087	

Table 2: Continued

No.	03	04	05	06	07	08	09	10	11	12	13	14	15
(1)	(2)	(3)	(4)	(5)	(6)	(7)	(8)	(9)	(10)	(11)	(12)	(13)	(14)
221	17.86	17.38	17.08	16.92	16.53	16.48	16.30	16.18	16.03	15.90	15.85	15.83	15.75
	0.016	0.012	0.011	0.010	0.010	0.009	0.010	0.011	0.014	0.011	0.019	0.019	0.025
222	18.20	17.82	17.64	17.50	17.28	17.26	17.08	17.00	16.86	16.82	16.77	16.58	16.51
	0.021	0.014	0.013	0.013	0.016	0.015	0.016	0.018	0.020	0.017	0.032	0.024	0.044
223	17.56	17.49	17.33	17.34	17.23	17.21	17.20	17.20	17.10	17.14	17.17	17.12	17.21
	0.022	0.026	0.029	0.026	0.033	0.032	0.039	0.040	0.049	0.047	0.073	0.074	0.118
224	16.22	15.92	15.67	15.54	15.28	15.24	15.10	15.02	14.92	14.83	14.80	14.77	14.76
	0.005	0.004	0.003	0.003	0.004	0.003	0.004	0.004	0.005	0.004	0.007	0.007	0.010
225	15.17	14.69	14.40	14.24	13.89	13.83	12.80	13.53	13.36	13.26	13.22	13.12	13.06
	0.004	0.003	0.003	0.002	0.002	0.002	0.001	0.002	0.002	0.002	0.003	0.002	0.003
228	17.96	17.44	17.09	16.92	16.55	16.44	16.25	16.13	15.95	15.82	15.85	15.75	15.67
	0.016	0.009	0.008	0.007	0.008	0.007	0.007	0.009	0.010	0.009	0.017	0.015	0.020
229	17.37	17.07	16.81	16.69	16.41	16.37	16.22	16.14	16.01	15.93	15.93	15.90	15.85
	0.014	0.011	0.011	0.010	0.011	0.010	0.009	0.010	0.012	0.011	0.020	0.017	0.025
231	18.14	17.76	17.45	17.36	16.98	16.94	16.79	16.70	16.58	16.46	16.44	16.39	16.35
	0.033	0.023	0.019	0.020	0.021	0.018	0.020	0.020	0.025	0.025	0.041	0.037	0.046
234	17.67	17.33	17.03	16.86	16.56	16.50	16.25	16.23	16.07	15.92	15.94	15.87	15.78
	0.046	0.030	0.027	0.020	0.019	0.018	0.020	0.015	0.015	0.015	0.017	0.019	0.029
235	17.18	16.84	16.56	16.40	16.10	16.02	15.85	15.78	15.53	15.39	15.40	15.32	15.22
	0.019	0.013	0.012	0.010	0.009	0.008	0.008	0.008	0.008	0.007	0.012	0.012	0.016

Table 3: Age Distribution of 172 GCs

No.	Metallicity (Z)	Age ([log yr])	No.	Metallicity (Z)	Age ([log yr])
(1)	(2)	(3)	(1)	(2)	(3)
326.....	0.00400	8.806	57.....	0.00040	9.778
328.....	0.00400	9.301	59.....	0.00400	9.740
332.....	0.00400	9.057	60.....	0.00040	9.760
333.....	0.02000	9.544	61.....	0.02000	9.362
9.....	0.00040	10.068	63.....	0.00400	9.845
11.....	0.00040	10.248	64.....	0.00040	10.279
14.....	0.00040	9.574	67.....	0.00040	9.544
15.....	0.02000	9.009	68.....	0.00400	9.574
17.....	0.00400	9.720	69.....	0.00400	9.279
21.....	0.02000	9.544	70.....	0.00400	9.544
23.....	0.00400	9.813	71.....	0.00400	10.301
25.....	0.00040	9.978	72.....	0.00400	10.297
27.....	0.00040	9.875	73.....	0.00400	9.845
28.....	0.00400	9.155	75.....	0.00040	9.760
29.....	0.02000	9.942	76.....	0.00040	9.740
30.....	0.02000	9.279	77.....	0.00040	10.137
31.....	0.00040	9.602	78.....	0.02000	10.272
32.....	0.00400	9.677	79.....	0.00400	9.602
33.....	0.00400	10.146	80.....	0.02000	10.297
34.....	0.00400	9.778	82.....	0.00400	9.796
36.....	0.00400	10.130	84.....	0.02000	10.301
37.....	0.00400	9.966	86.....	0.00040	9.903
38.....	0.00400	9.322	88.....	0.00040	10.021
39.....	0.00400	9.796	90.....	0.02000	9.009
41.....	0.00400	10.013	91.....	0.00040	9.207
42.....	0.00040	10.267	92.....	0.00040	9.720

Table 3: Continued

No.	Metallicity (Z)	Age ([log yr])	No.	Metallicity (Z)	Age ([log yr])
(1)	(2)	(3)	(1)	(2)	(3)
101.....	0.02000	9.301	141.....	0.00400	9.439
103.....	0.00400	10.130	143.....	0.00400	10.155
102.....	0.00040	9.699	144.....	0.00400	10.021
104.....	0.00040	9.574	145.....	0.02000	10.272
105.....	0.00400	9.796	146.....	0.02000	9.279
106.....	0.00400	9.796	148.....	0.00040	10.176
108.....	0.00400	8.957	149.....	0.00040	9.929
107.....	0.00040	9.875	150.....	0.02000	9.255
109.....	0.02000	9.544	151.....	0.00400	9.860
111.....	0.00040	10.196	152.....	0.02000	9.362
110.....	0.00400	9.574	153.....	0.00400	10.301
112.....	0.02000	9.860	154.....	0.00040	9.255
114.....	0.02000	9.107	155.....	0.02000	9.477
117.....	0.00040	10.033	157.....	0.00040	9.544
115.....	0.00400	10.297	158.....	0.00400	9.699
116.....	0.00400	9.978	159.....	0.00040	10.301
118.....	0.00040	9.740	160.....	0.00400	9.255
122.....	0.00400	10.301	161.....	0.00040	10.155
123.....	0.00400	9.929	162.....	0.02000	9.342
125.....	0.00040	9.796	163.....	0.00400	10.301
126.....	0.00040	10.297	164.....	0.02000	9.009
127.....	0.00400	9.813	165.....	0.00400	9.322
353.....	0.02000	10.301	166.....	0.00040	9.301
128.....	0.00040	10.301	167.....	0.00400	10.155
130.....	0.00040	10.041	169.....	0.00400	9.322
131.....	0.00400	10.283	171.....	0.00400	10.155

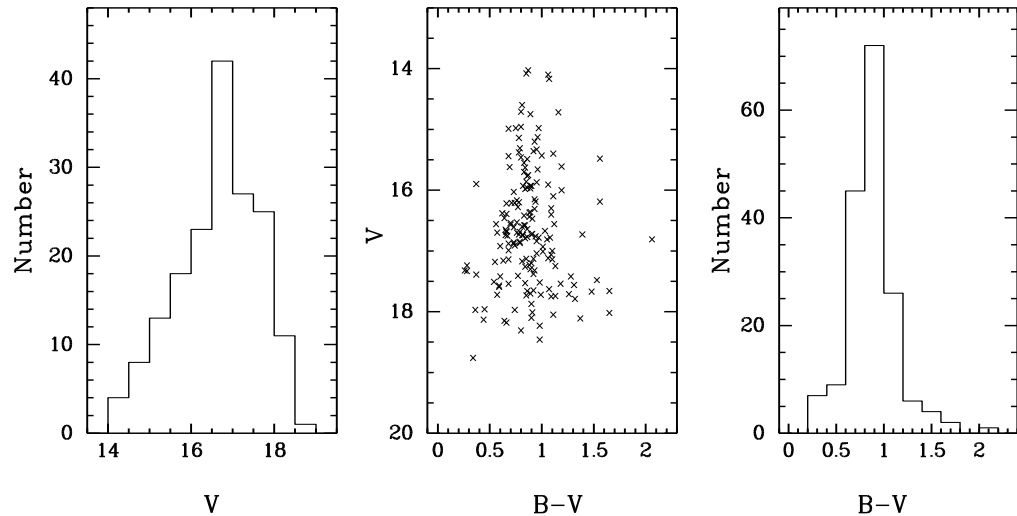


Fig. 1.— Histograms of the computed V magnitudes and B-V colors, and color-magnitude diagram, for 172 GCs

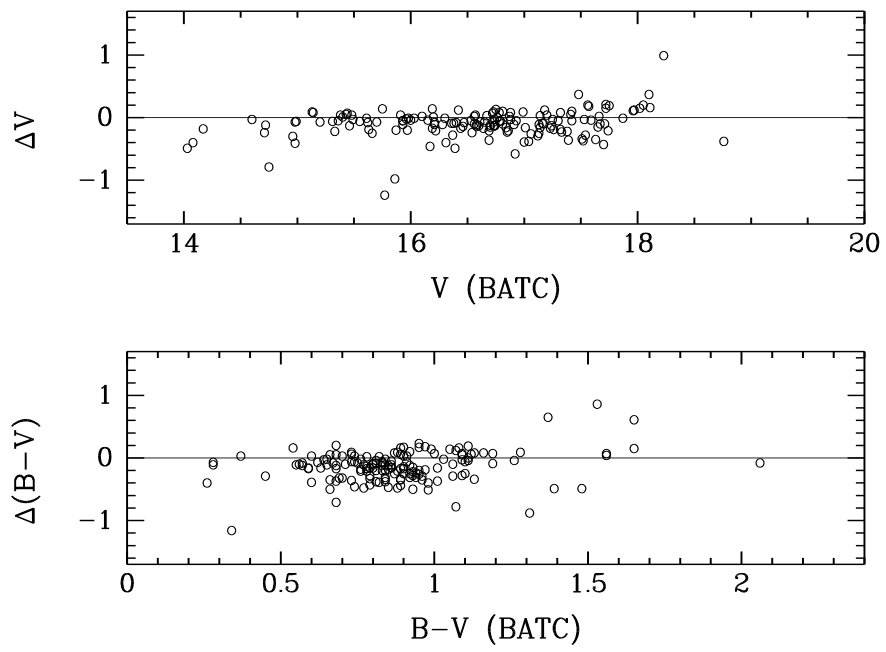


Fig. 2.— Comparison of GC photometry with Battistini et al. (1987). The vertical axis is the BATC photometry minus the measurement of Battistini et al. (1987).

Table 3: Continued

No.	Metallicity (Z)	Age ([log yr])	No.	Metallicity (Z)	Age ([log yr])
(1)	(2)	(3)	(1)	(2)	(3)
180.....	0.00040	10.041	208.....	0.00400	9.845
181.....	0.00400	9.477	209.....	0.00400	9.677
182.....	0.00400	9.720	210.....	0.00400	9.107
183.....	0.00400	10.000	211.....	0.00040	10.301
185.....	0.00400	9.760	213.....	0.00400	9.628
184.....	0.00400	9.477	214.....	0.00040	10.283
186.....	0.02000	10.301	215.....	0.00400	10.061
187.....	0.00040	10.090	216.....	0.00040	8.957
188.....	0.00400	10.283	362.....	0.00040	6.620
189.....	0.02000	9.845	217.....	0.00400	9.720
190.....	0.00400	9.813	218.....	0.00040	10.301
192.....	0.00040	9.255	220.....	0.00040	10.079
194.....	0.00040	10.301	221.....	0.00040	10.301
193.....	0.00400	10.301	222.....	0.02000	9.107
197.....	0.00040	9.057	223.....	0.00040	8.806
198.....	0.00400	9.889	224.....	0.00040	9.860
200.....	0.00040	9.875	225.....	0.00400	9.966
201.....	0.00400	9.778	228.....	0.00400	10.090
203.....	0.00040	10.297	229.....	0.00400	9.699
204.....	0.00400	9.574	231.....	0.00400	9.929
205.....	0.00400	9.740	234.....	0.00400	9.628
206.....	0.00400	9.628	235.....	0.00400	9.778

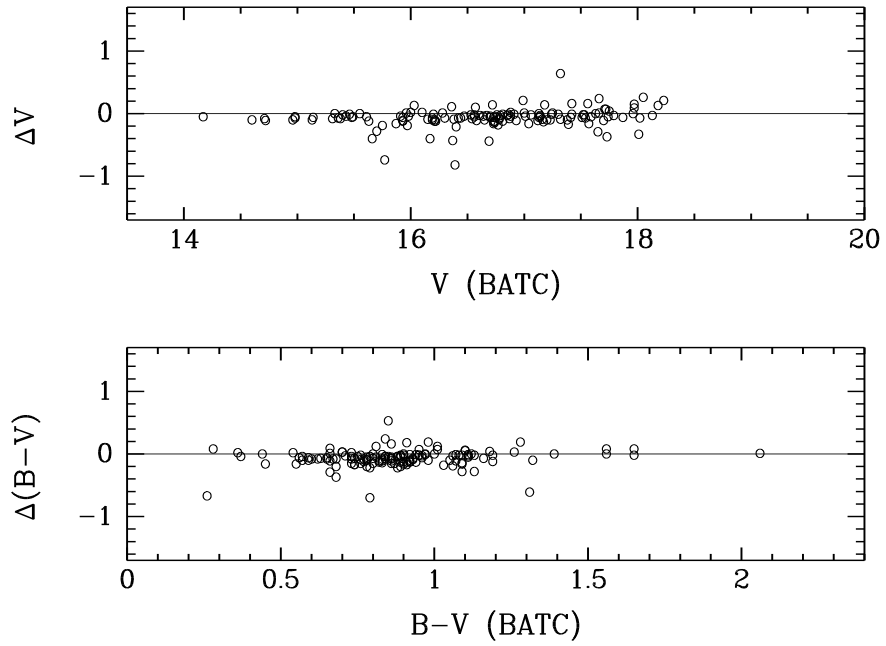


Fig. 3.— Comparison of GC photometry with Barmby et al. (2000). The vertical axis is the BATC photometry minus the measurement of Barmby et al. (2000).

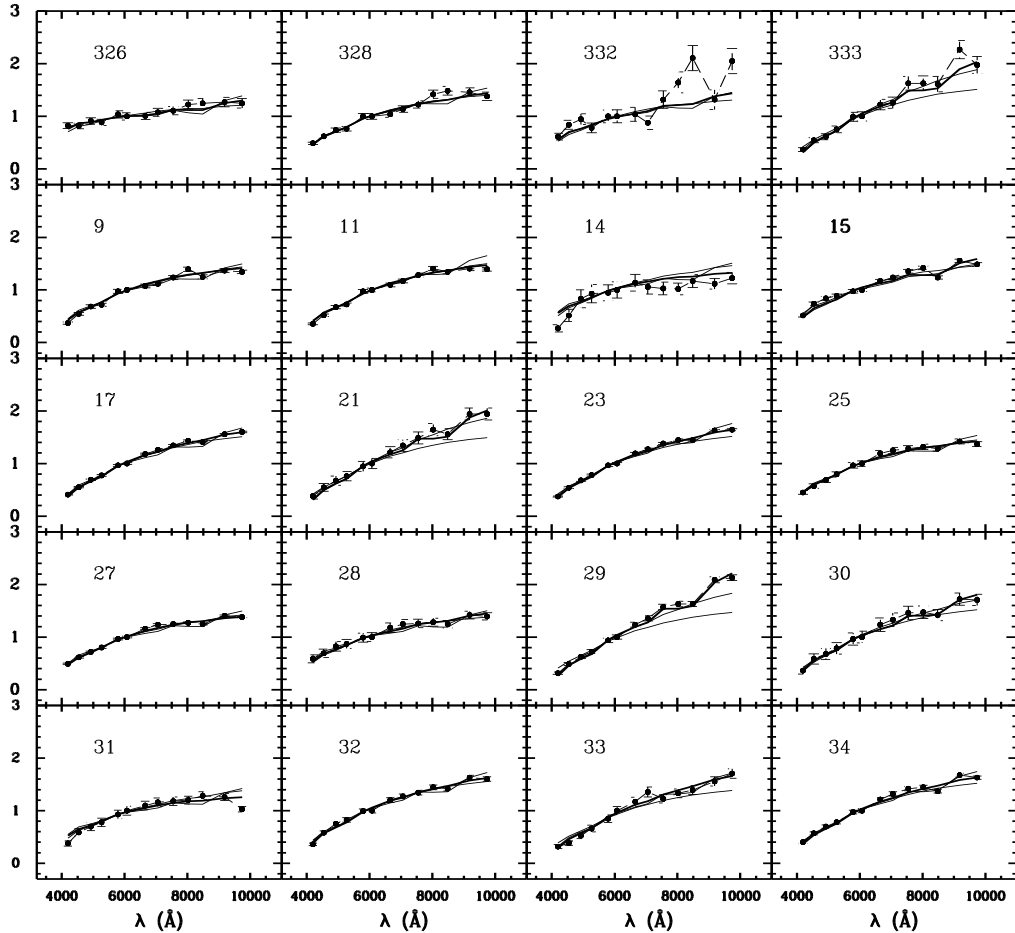


Fig. 4.— Map of the fit of the integrated color of a SSP ($Z = 0.0004, 0.004$, and 0.02) with intrinsic integrated color for 20 GCs selected from the 172 GCs (the first 20 GCs in Table 2). Filled circle represents the intrinsic integrated color of a GC, the thick line represents the best fit of the integrated color of a SSP of GSSP, and the thin lines represent the other two fits. Y-axis is the ratio of the flux in each filter to the flux in filter BATC08.

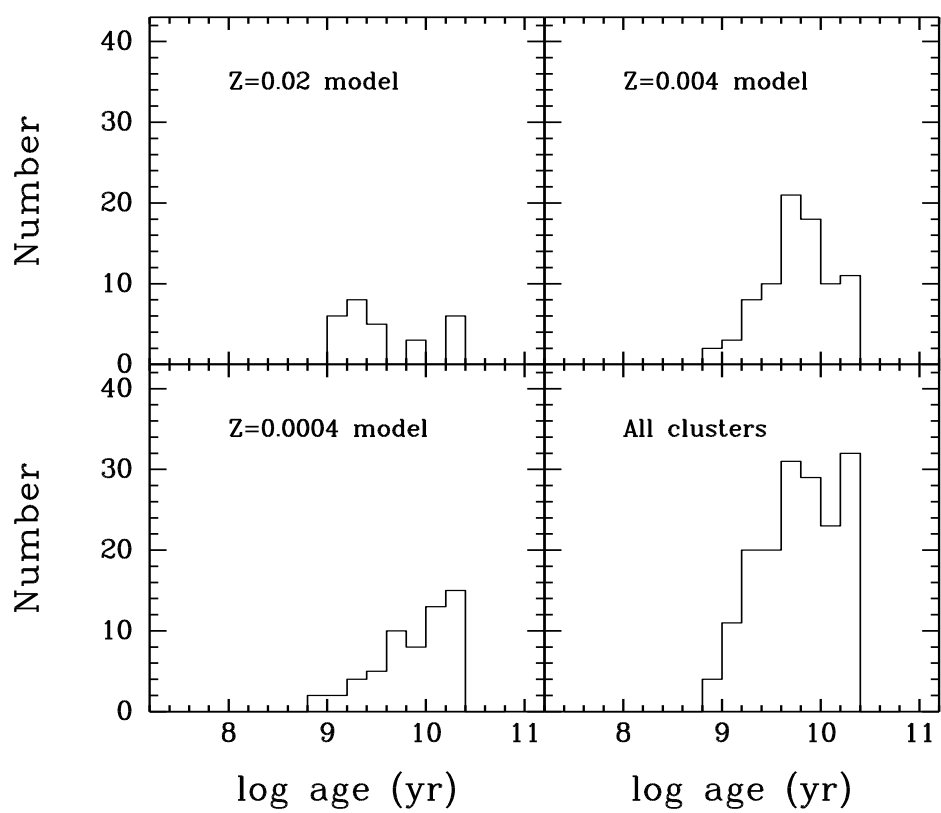


Fig. 5.— Histograms of M31 GC ages

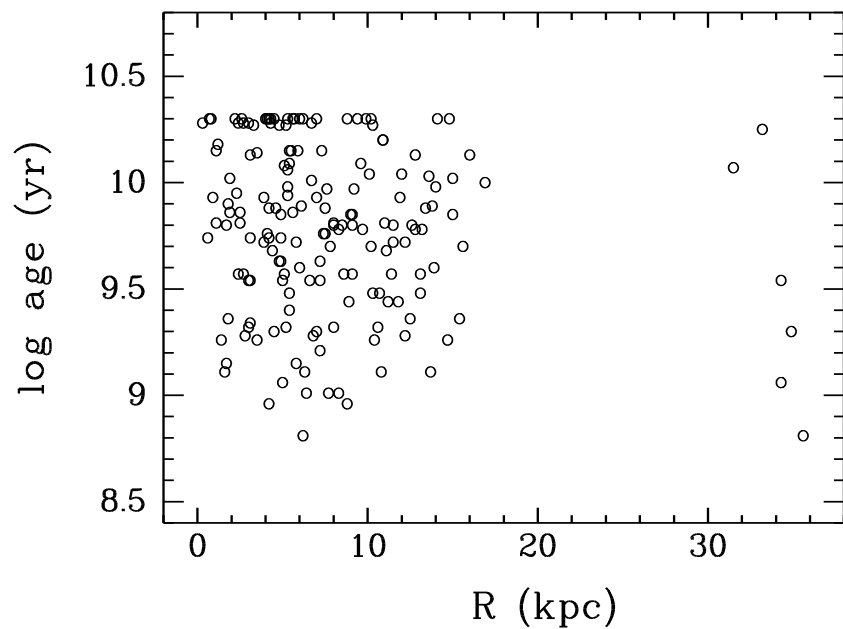


Fig. 6.— Age as a function of galactocentric distance for M31 GCs. The absence of GCs with $20 < R < 30 \text{ kpc}$ is a selection effect.

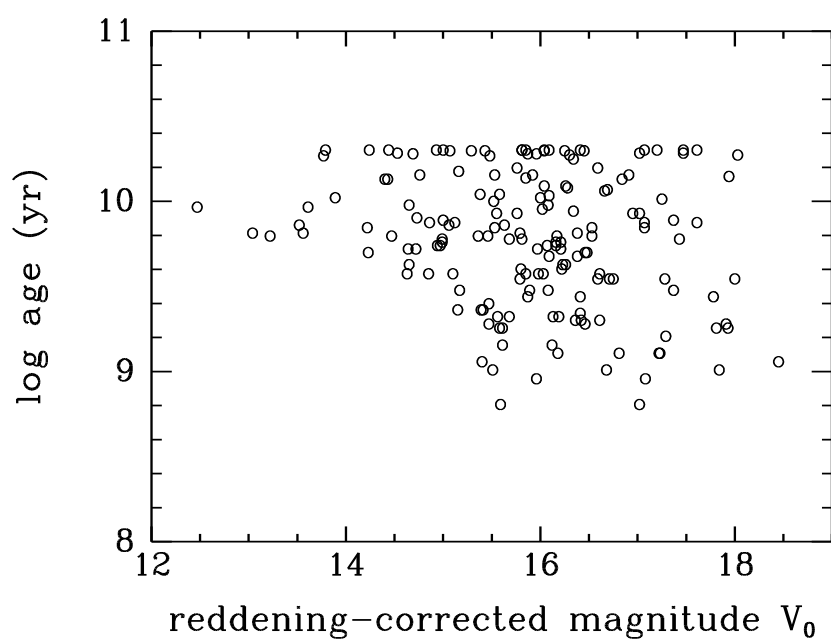


Fig. 7.— Age as a function of reddening-corrected magnitude V_0 for M31 GCs